LONGITUDINAL FACE CRACK PREDICTION WITH THERMO-MECHANICAL MODELS OF THIN SLABS IN FUNNEL MOULDS

L. C. Hibbeler,B. G. Thomas, B. Santillana, A. Hamoen, A. Kamperman

This paper investigates longitudinal depressions and cracks in steel continuous-cast in funnel moulds using a finite-element model to simulate thermo-mechanical behavior of the solidifying shell in the thin-slab caster mould at the Corus Direct Sheet Plant (DSP) in IJmuiden, The Netherlands. The commercial code ABAQUS [1] is used to study the effect of the funnel shape on the stresses developed within a two-dimensional section through the shell while it moves through the mould. The model first simulates heat transfer, based on heat flux profiles found from extensive plant measurements of mould heat removal and thermocouples embedded in the mould wall. It incorporates the drop in heat flux due to local gap formation. The temperature solution is input to the mechanical model which incorporates grade-dependent elastic-viscoplastic constitutive behavior, ferrostatic pressure, taper, mould-wall oscillations, and contact with the profiled mould wall. The results are validated with plant measurements, including a breakout shell, and crack statistics. The model is applied to study the effects of increasing casting speed and funnel design in order to avoid longitudinal cracks.

KEYWORDS: funnel mould, longitudinal face crack, thin-slab casting, continuous casting, numerical model

INTRODUCTION

Longitudinal face cracks are one of many problems that can arise in thin-slab continuous casting. They can be caused by a variety of sources, including non-uniform heat transfer, mould level fluctuations, inadequate taper, excessive taper, and problems with the funnel shape. Funnel molds have a fundamental difference from other continuous casting molds in that the shape of the cross section from mold top to mold bottom changes significantly. Funnel molds currently in use in industry have as much as 60 mm difference in the position of the hot face from top to bottom, which represents more than half of the steel strand thickness. This contrasts with conventional slab, beam blank, or billet casters, which have differences of only a few millimeters, due to taper or casting-machine radius. This large change in dimensions is responsible for inducing extra bending effects in the shell, which can cause new defects and worsen existing problems.

Lance C. Hibbeler
University of Illinois at Urbana-Champaign, USA
Brian G. Thomas
University of Illinois at Urbana-Champaign, USA
Begoña Santillana
Corus RD&T SCC/CMF, The Netherlands
Arie Hamoen
Corus RD&T SCC, The Netherlands
Arnoud Kamperman
Corus Strip Products IJmuiden/Direct Sheet Plant, The Netherlands

Paper presented at the European Conference Continuous Casting of Steel, Riccione, 3-6 June 2008, organised by AIM

A specific type of longitudinal defect, called a depression, is shown in Fig. 1. Severe depressions also contain an intermittent crack, which exhibit a, random zig-zag shape, running along austenite grain boundaries. These cracks have similar appearance to longitudinal facial cracks in conventional slabs, whose formation mechanisms are reviewed by Brimacombe and coworkers

Fig. 1 ***Depression Longitudinal Face Crack.***
Cricca superficiale longitudinale con depression.

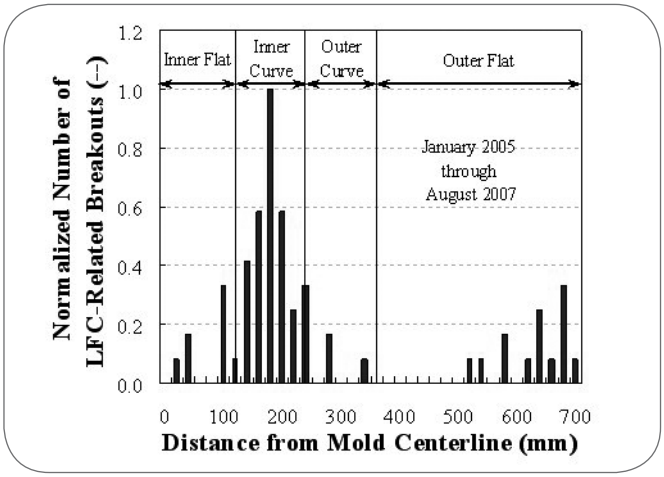

Fig. 2

Locations of LFC-Related Breakouts.

Posizione dei difetti dovuti a cricche superficiali longitudinali.

[2]. Longitudinal depressions generally initiate at the meniscus. For example, a depression can start from a small level fluctuation causing a localized variation in the thickness of solidified slag rim, such as a slag "finger" that extends slightly below the meniscus between the shell and the mold. The corresponding local drop in heat transfer, and locally hot and thinner shell in that region might grow into a deeper depression, if the defect is located in a susceptible region of the funnel that causes extra bending stress, which buckles the shell into the melt. This could increase the gap size, leading to further local thinning of the shell and longitudinal crack formation. If conditions aggravate the depression as it moves down the mold, this can cause a worst-case scenario, a breakout, at mold exit. Alternatively, subsurface cracks have been suggested to propagate to the surface due to reheating below the mold, again causing surface cracks and breakouts [2]. The relative importance of the meniscus and lower mold shape on the problem, and the details of the mechanism of longitudinal depression formation have not been quantified previously.

Several researchers have developed computational models of the thermo-mechanical behavior of solidifying shells in the mold of conventional slabs [2], beam blanks [7,15] and billets [6,18]. Konishi recently applied numerical models to investigate mid-face LFCs related to the delta-to-gamma phase transformation, and advocates that the uniformity of heat transfer in the meniscus region is of utmost importance, regardless of the magnitude of the heat flux [11]. Li modeled the formation of off-corner longitudinal cracks in billets [16], and Park studied corner cracks [18] as a function of corner radius. Heat transfer in thin-slab casters has been analyzed in previous work [3,18,22]. Funnel mold distortion was modeled by O'Connor [17], but to date there has been little work done to study longitudinal crack formation in steel cast in funnel molds, which is the subject of this study.

PLANT EXPERIENCE

A database of breakouts has been maintained at the Corus DSP since 2005, which details many of the circumstances of all breakouts, including the location of the breakout, the casting conditions, mold heat flux, and thermocouple measurements. A histogram of the location of the breakouts resulting from longitudinal facial cracks is shown in Fig. 2. This mold exhibits a strong tendency for longitudinal cracks forming in the area called the "inner curve," explained in the next section. All of the cracks in the central region of the mold are clearly recognized by very deep depressions, up to 20 mm deep. Fig. 2 also shows evidence of off-corner longitudinal cracks, referred to as "Craquelet," which do not have the accompanying depressions. The steel grades of interest are low-carbon hypoperitectic steels, such as the typical plain-carbon steel with 0.045%C modeled.

FUNNEL MOULD GEOMETRY AND ANALYSIS DOMAIN

The funnel design analyzed in this work is shown in Fig. 3. In the horizontal plane, the funnel shape is defined by two tangent circles of opposite curvature between two flat parallel regions. The inner flat region consists of the center 260 mm of the wide face, and the outer flat region stretches from 375 mm from the center of the wide face to the outer edge of the copper plate. Although the mold is 1860 mm wide, the strand width adopted in this domain is 1200 mm (measured at mold exit). In the vertical plane, the funnel is a large arc from the top of the mold to 850 mm down the 1100-mm-long mold. Below this, the mold walls become vertical. The "crown" of the funnel, half the difference between the strand thicknesses at the centerline and near the narrow face, is 23.4 mm at the top of the mold and 8 mm at 850 mm below mold top and lower. The mold profile at mold exit still has a small amount of curvature, requiring specially shaped rollers at the beginning of secondary cooling.

The computational analysis domain used for this work takes advantage of quarter symmetry, and includes a 20-mm thick strip of the strand region, and a small strip of the copper mold. The steel strip is about twice the expected shell thickness at mold exit and includes both the solidifying shell and a portion of the internal liquid. The thin-strip-shaped domain eases computation, as the liquid steel behavior is not of great interest to longitudinal face cracking.

NUMERICAL MODEL OF CONTINUOUS CASTING OF STEEL

A computational model of heat transfer and stress in the solidifying steel shell was developed at the University of Illinois and applied in this work to simulate the thermo-mechanical behavior of a two-dimensional (2D) transverse slice through the shell, as it moves down through the mold at the casting speed. The domain is highlighted in Fig. 3.

The process of continuous casting of steel has a large Peclét num-

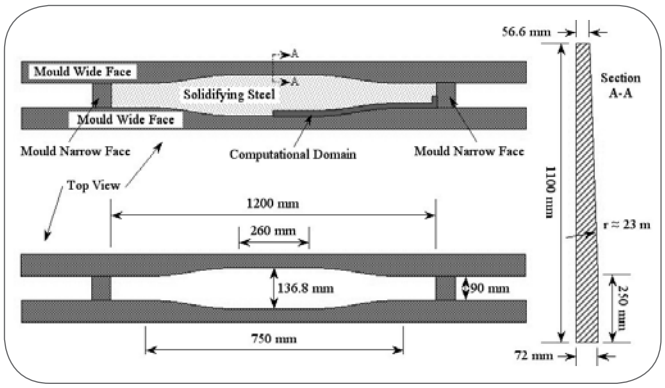

Fig. 3

Funnel Mould Geometry.

Geometria della lingottiera a imbuto.

ber, (casting speed * thickness / thermal diffusivity), so the axial (casting) direction heat conduction is negligible. The appropriate corresponding assumption for the 2D mechanical analysis is generalized plane strain, where all of the nodes in the axial direction are constrained to move together as a flat plane with constant thickness. Recent numerical modeling with a three-dimensional transient model has shown this 2D assumption to be accurate throughout the mold region [12]. This two-dimensional assumption cannot accurately capture the out-of-plane bending stresses, such as those that occur at the transition 850 mm below the top of the mold. Fortunately, this effect is of little consequence in this work, where the transverse stresses and strains control the longitudinal depressions and cracks.

The material properties of steel vary with temperature and carbon content, according to measurements of elastic modulus [20], thermal conductivity [4], specific heat capacity [5], and density [4,5,10]. The coefficient of thermal expansion can be calculated easily from the density [13]. Each of these property models were included in the thermo-mechanical simulation for the 0.045 % wt. C steel that is cast at the Corus DSP. The density was maintained at a constant 7500 kg/m3 to conserve mass. For the sake of simplicity, all material properties are modeled as isotropic, which neglects any influence of the orientation of the columnar-grained microstructure.

Separate constitutive models are adopted for the liquid, delta-ferrite, and austenite phases. The liquid and mushy regions are treated as an elastic-perfectly plastic solid with a very low elastic modulus, and very low yield stress. For austenite, the Kozlowski et al. model III [14] is used, which fits tensile-test data from Wray [26] and creep-test data from Suzuki [23] :

$$\dot{\bar{\varepsilon}}_{ie}\left[\sec^{-1}\right] = f_C\left(\bar{\sigma}[\mathrm{MPa}] - f_1\,\bar{\varepsilon}_{ie}\,|\bar{\varepsilon}_{ie}|^{f_2-1}\right)^{f_3}\exp\left(-\frac{Q}{T[\mathrm{K}]}\right)$$

where :

$$Q = 44,465$$

$$f_1 = 130.5 - 5.128\times10^{-3}T\,[\mathrm{K}]$$

$$f_2 = -0.6289 + 1.114\times10^{-3}T\,[\mathrm{K}]$$

$$f_3 = 8.132 - 1.54\times10^{-3}T\,[\mathrm{K}]$$

$$f_C = 46,550 + 71,400\,(\%C) + 120,000\,(\%C)^2 \qquad (1)$$

This empirical relation relates the equivalent inelastic strain rate $\dot{\bar{\varepsilon}}_{ie}$ with the von Mises stress $\bar{\sigma}$, equivalent inelastic strain $\bar{\varepsilon}_{ie}$, activation constant Q, carbon content %C, and several empirical temperature- or steel-grade-dependent constants f_1, f_2, f_3, and f_c.

The delta-ferrite phase exhibits significantly higher creep rates and lower strength than the austenite phase, so the following a power-law constitutive relation for the delta-ferrite phase from Zhu [27] is used, which is also based on fitting measurements at higher temperature:

$$\dot{\bar{\varepsilon}}_{ie}\left[\sec^{-1}\right] = 0.1\left|\frac{\bar{\sigma}[\mathrm{MPa}]}{f_{\delta c}(\%C)\left(\frac{T[\mathrm{K}]}{300}\right)^{-5.52}(1+1000\bar{\varepsilon}_{ie})^m}\right|^n$$

where :

$$f_{\delta c}(\%C) = 1.3678\times10^4\,(\%C)^{-5.56\times10^{-2}}$$

$$m = -9.4156\times10^{-5}T[\mathrm{K}] + 0.3495$$

$$n = \frac{1}{1.617\times10^{-4}T[\mathrm{K}] - 0.06166} \qquad (2)$$

Two-phase regions containing mixtures of ferrite and austenite are treated as delta whenever more than 10% by volume delta-ferrite is present. This roughly incorporates the dominating effect of the high-creep rate of delta-ferrite on the overall material response. The convergence problems associated with these two highly nonlinear elastic-viscoplastic constitutive models are overcome using a special two-level local-global iteration scheme [13], that was implemented into ABAQUS 6.7 [1] through the user-defined subroutine UMAT.

Mechanical contact between the curved surface of the funnel mold and the solidifying shell poses little problem for the vector-based contact algorithms in ABAQUS. This mechanical contact was treated with a "softened" exponential pressure-overclosure relationship to aid convergence. The tangential friction coefficient was a uniform = 0.16, which is based on friction measurements [19] of solidified slag on copper.

Ferrostatic pressure is applied as a distributed load that linearly increases with time (distance down the mold) as illustrated in Fig. 4. Ferrostatic pressure is computationally challenging because the soft mushy elements cannot sustain any significant mechanical load. Instead of the load pushing on the inside surface of the shell, the ferrostatic pressure is applied on the outside surface of the shell, pulling the steel towards the mold. This slight change in location does not effect the mechanical behavior of the shell very much. In addition, the onset of ferrostatic pressure is delayed slightly less than one second in order to allow most of the outermost layer of elements to become completely solidified. These changes to ferrostatic pressure greatly aid convergence.

The analysis is performed in two steps, consisting of a heat transfer analysis from meniscus to mold exit, and then a mechanical analysis, from meniscus to mold exit. Although this neglects the strong nonlinear coupling between the heat transfer and interfacial gap size, this "one-way coupled" analysis is accurate in regions of good contact and helps to ensure a stable analysis. The heat flux profile used in regions of good contact is given in Fig. 4. The heat flux profile was simplified to a monotonically-decreasing curve to aid convergence, but the average value of the profile matches measurements of mold water heat-up in the plant. Regions of gap formation are assigned heat transfer values based on the expected behavior, which must be checked after the analysis. Specifically, heat flux near the corner was linearly decreased to half of its nominal value over a 20 mm zone at the corner.

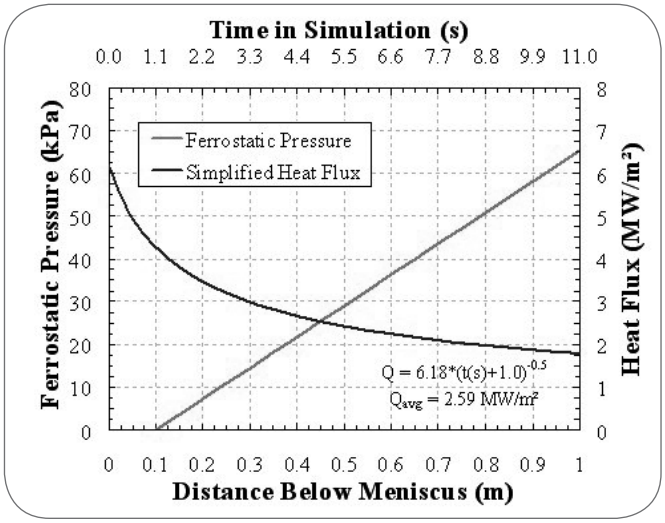

Fig. 4 ***Ferrostatic Pressure and Heat Flux.***
Pressione ferrostatica e flusso di calore.

In another simulation, the local heat transfer in a 30-mm region was decreased linearly to 50% in the center in order to initiate a longitudinal depression / local gap formation and shell thinning. Buckling was facilitated by neglecting the local ferrostatic pressure in that region, in order to avoid numerical instabilities caused by over-center bending towards the mold wall.
Transformation from three dimensions to two dimensions and time is needed to include the heat transfer and displacement boundary conditions. With a constant casting speed, the relation from the axial (z) coordinate to time for the steel shell is:

$$z_{shell}(t) = z_{meniscus} + V_c t \quad (3)$$

where z_{shell} is the distance below the mould top, $z_{meniscus}$ is the depth of the meniscus, V_c is the casting speed, and t is the time in the two-dimensional simulation. The domain moves through the mould with the same relationship, and an extra term can include the effect of (sinusoidal) oscillation:

$$z_{mold}(t) = z_{meniscus} + V_c t + \frac{S_{osc}}{2}\sin(2\pi f_{osc} t) \quad (4)$$

where S_{osc} is the stroke (peak-to-peak) of the mould oscillations and f_{osc} is the oscillation frequency in Hz. Displacement functions are applied to the mould surface nodes to accurately recreate what the two-dimensional slice experiences as it moves down the mould hot face. A linear narrow face taper was included by defining the following fixed-displacement conditions to the hot face, relative to its initial position at the meniscus:

$$u_{NF}(t) = \Delta \frac{z_{mold}(t) - z_{meniscus}}{L_{mold}} \quad (5)$$

where u_{NF} is the narrow face displacement function, Δ is the narrow face taper in units of length per side, and L_{mold} is the mould length. These displacement functions are included in the model as time-dependent boundary conditions for each region of the mould. Two examples of these functions are given in Fig. 5. Mould distortion was neglected from these boundary conditions.
The casting speed used in this work is 5.5 m/min, the oscillation frequency and stroke are 5.52 Hz and 7.2 mm, respectively, and the meniscus depth is 104 mm (based on measurements), giving a time in mould of 10.86 seconds.

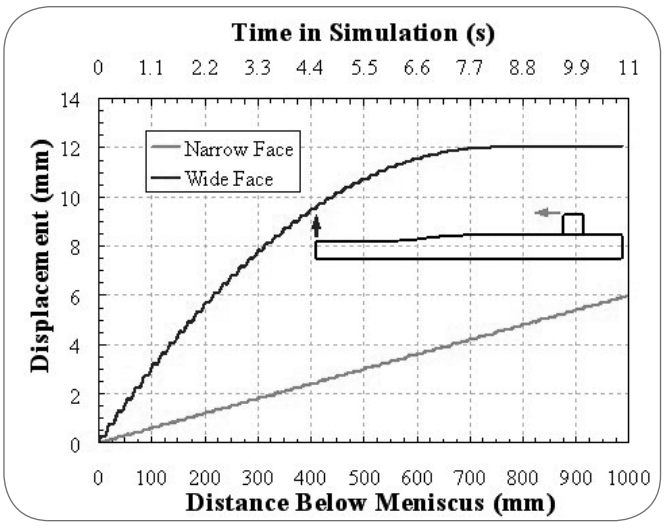

Fig. 5

Mould Displacement Functions.
Funzioni di spostamento dello stampo.

The heat transfer analysis was solved using the enthalpy method in ABAQUS to incorporate latent heat evolution from the liquid to solid phase change [9]. The numerical solution scheme is modified at early iterations to aid convergence [1]. The effects of composition, cooling rate, and microsegregation [25] on the heat transfer were coupled into the model directly through the temperature dependence of the material properties via the phase diagram during pre-processing. The stress analysis was solved with ABAQUS/Standard (implicit solution technique) using generalized plane-strain with the user-defined UMAT. To achieve reasonable accuracy, the domain featured a refined mesh with elements less than 1-mm thick on the surface. The stress analysis required just over 30 hours (wall clock) on NCSA's Xeon Linux cluster computer (using four processors) for the two-dimension domain of 17130 nodes and 17258 elements (51797 total degrees of freedom).
The components of all tensor field variables (stresses and strains) reported in this work were transformed to a plane tangent to the mould surface, using elementary solid mechanics relations [8] and understanding the mould geometry during post processing. These "tangential" values are very close to values on the plane perpendicular to the dendrite growth direction and are of primary interest because they are the cause of longitudinal cracking. The corresponding values in the casting direction are quite similar to the tangential values, and are not presented. The stresses in the dendrite growth direction are very small during solidification in the mould.

MODEL VERIFICATION

The numerical models are verified with analytical solutions to ensure that the model can capture accurately the fundamental thermo-mechanical phenomena. Consider a pure material (or eutectic alloy), initially at its freezing temperature, solidifying as an unconstrained, elastic, perfectly plastic plate. The analytical solution to this problem was first derived by Weiner and Boley [24] in 1963. One edge of this plate suddenly comes into perfect contact with an isothermal wall at a specified temperature, and solidification begins immediately. All material properties are constant with temperature except the yield stress, which decreases linearly to zero at the freezing temperature. The temperature distribution and three-dimensional state of stress of this problem can be modeled accurately with a single row of finite elements with a generalized plane strain condition imposed in the other two directions. A 30×0.1 mm strip through the thickness of the plate was chosen as the analysis domain, as shown in Fig. 6, and the material properties and problem parameters are tabulated in Tab. 1. To make the problem more amenable to numerical solution, adjustments were made, including a small mushy zone, adding a small superheat, having a small (35 kPa) yield stress at the solidus temperature,

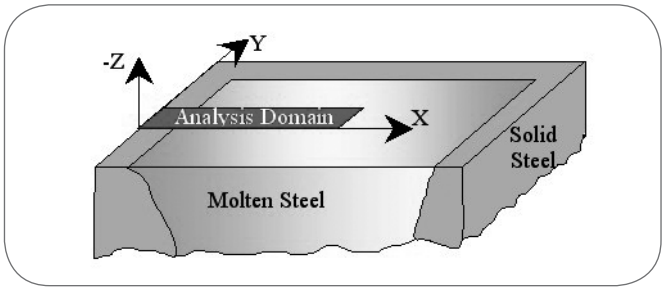

Fig. 6

Verification Problem Domain.
Zona di verifica del problema.

Property/Parameter	Value	Units
Mass Density, ρ	7500	kg/m3
Specific Heat Capacity, C_p	661	J/(kg· °C)
Latent Heat of Fusion, L_f	272	kJ/kg
Thermal Conductivity, k	33	W/(m· °C)
Thermal Expan. Coefficient, α	20·10-6	m/(m·°C)
Poisson's Ratio, υ	0.3	–
Elastic Modulus of Solid, E_s	40	GPa
Elastic Modulus of Liquid, E_l	14	GPa
Yield Stress at Surf. Temp., σ_Y^0	20	MPa
Initial Temperature, T_0	1495.0	°C
Liquidus Temperature, T_{liq}	1494.48	°C
Solidus Temperature, T_{sol}	1494.38	°C
Surface Temperature, T_{surf}	1000.0	°C

Tab. 1

Verification Problem Parameters.

Parametri utilizzati per la verifica.

and decreasing the elastic modulus to a smaller value in the liquid elements to consume any thermal strain developed in the liquid as the superheat flows out of the domain. The analytical and numerical results are presented in Figs. 7 and 8, both of which show favorable agreement at several times after the onset of solidification.

THROUGH-THICKNESS RESULTS

With the model thus verified, it was applied to simulate shell behavior in the funnel mould. To examine further the behavior through the shell thickness, a separate simulation with a fine meshed one-dimensional domain was performed. The results of this simulation are representative of the transverse tangential values found in the funnel mould away from corners and in the funnel transition region. The temperature, stress, and strain profiles are presented in Figs. 9, 10, and 11, and histories of strain, temperature, and

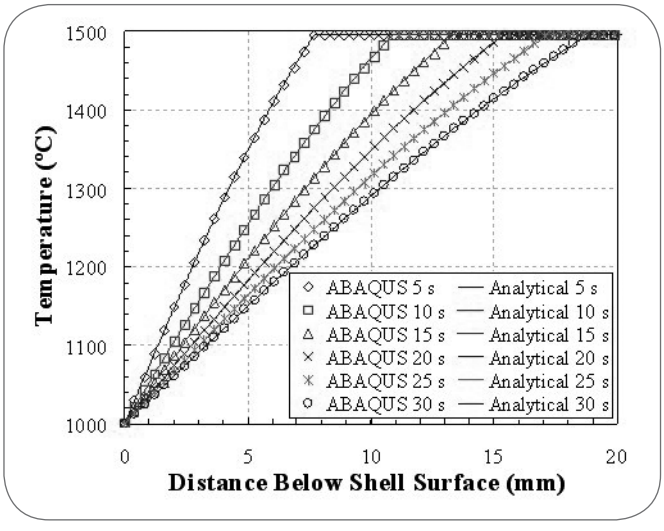

Fig. 7

Verification of Temperature Field.

Verifica del campo di temperature.

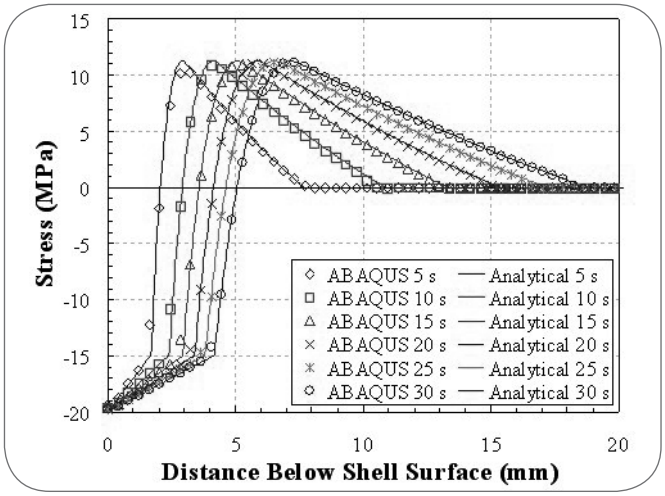

Fig. 8

Verification of Stress Field.

Verifica del campo di tensioni.

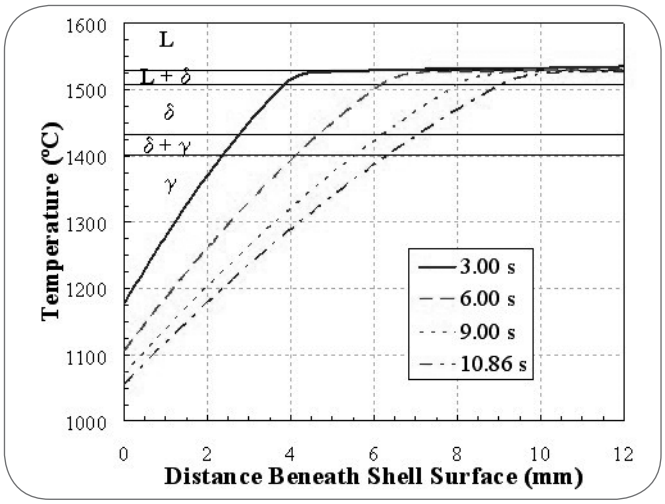

Fig. 9

Realistic Temperature.

Temperatura realistica.

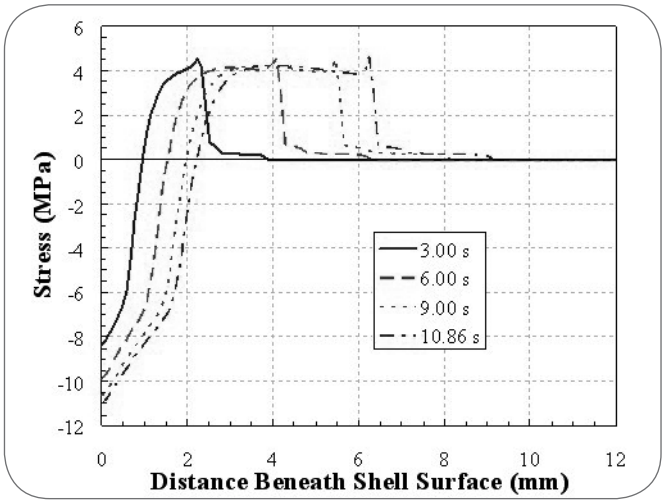

Fig. 10

Realistic Transverse Tangential Stress.

Tensione tangenziale trasversale realistica.

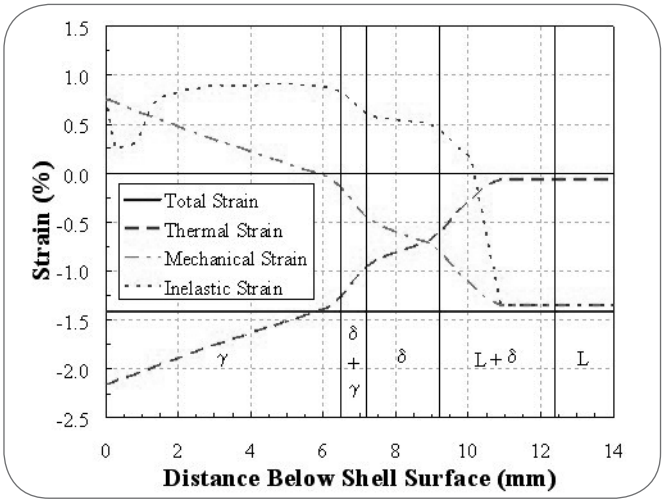

Fig. 11

Realistic Transverse Strain at Mould Exit.

Deformazione trasversale realistica all'uscita dello stampo.

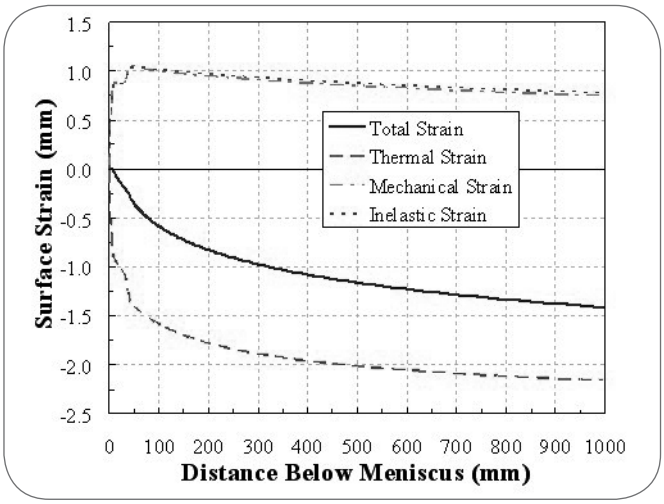

Fig. 12

Surface Strain History.

Andamento della deformazione superficiale.

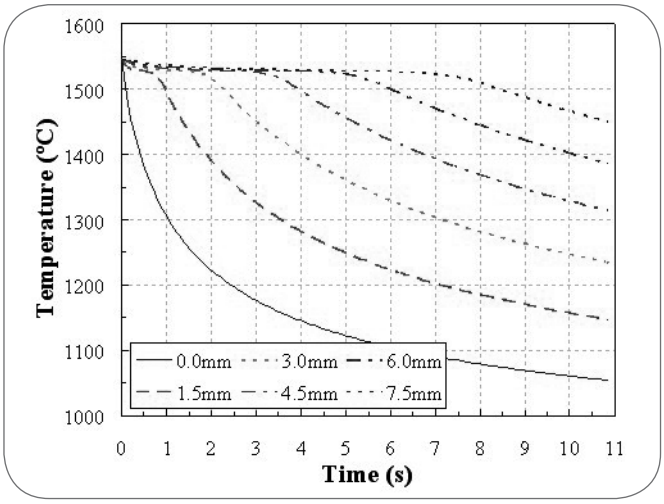

Fig. 13

Realistic Temperature Histories.

Andamento realistico della temperatura.

stress in Figs. 12, 13, and 14. The temperature profiles exhibit similar qualitative behavior as the analytical solution, except that the surface temperature gradually drops with time. The surface is initially in tension, but becomes compressive suddenly around 0.5 seconds when austenite first forms, and this stronger material can then sustain an appreciable load. The sharp transitions between the elastic and plastic regimes in the analytical solution profiles are not present with the realistic viscoplastic constitutive model.

The total strain within the one-dimensional slice domain can be broken down into its constituent parts, including the thermal, inelastic, and elastic strains. The "mechanical" strain is defined as the thermal strain subtracted from the total strain, and is useful in understanding the driving force for stress. As shown in Fig. 11, the overall shrinkage induces a negative total strain, which of course must be constant throughout the thickness. The extra thermal shrinkage at the surface is offset by tensile inelastic strain. As solidification progresses, the temperatures drop slower towards the interior, as shown in Fig. 13. This causes a decreasing temperature gradient through the shell, which generates internal tension (near the solidification front). This is offset by increasing compressive stress at the surface, as shown in Figs. 10 and 12, so that the total stress through the section is negligible.

These results provide a great deal of insight into the nature of the thermo-mechanical behavior of solidifying steel in a continuous caster. They also elucidate the effect of grade dependent phase changes: the additional thermal contraction from delta-ferrite to austenite, shown in Fig. 11, causes extra inelastic tensile strain and stress just below the solidification front. Fig. 14 shows that this tension peak appears at later times (further down the mould) at deeper distances beneath the shell surface. Each location in the surface third of the shell eventually goes into compression.

RESULTS AROUND THE PERIMETER

The funnel changes the classic thermo-mechanical behavior described in the previous section. Firstly, the curvature makes a very small two-dimensional contribution to the heat transfer in the funnel region, which causes surface temperature chan-

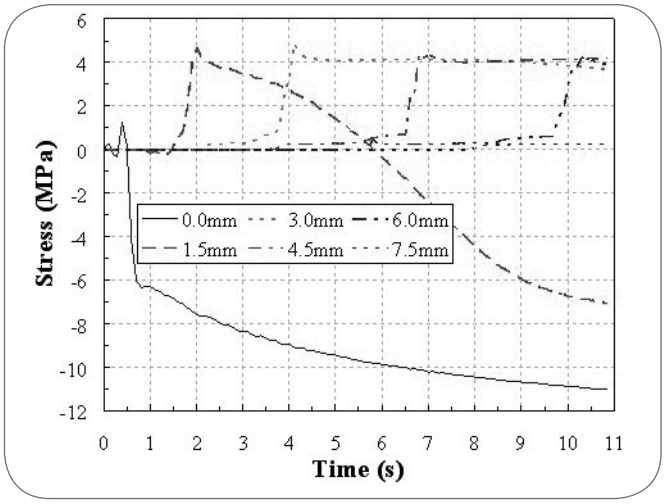

Fig. 14

Realistic Stress Histories.

Andamento realistico delle tensioni.

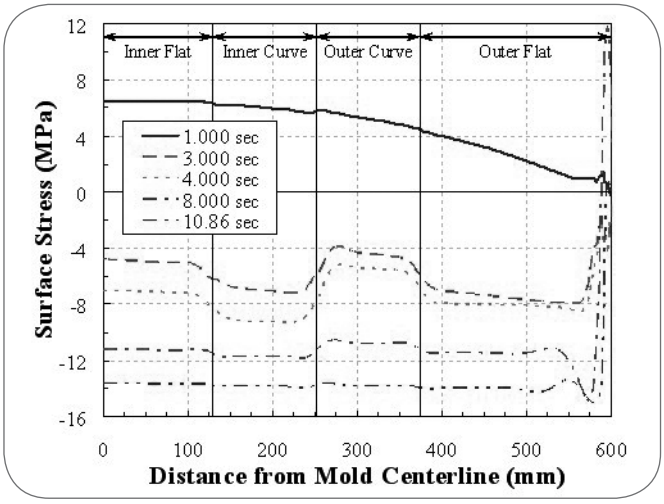

Fig. 15

Stress Around the Perimeter.

Tensione attorno al perimetro.

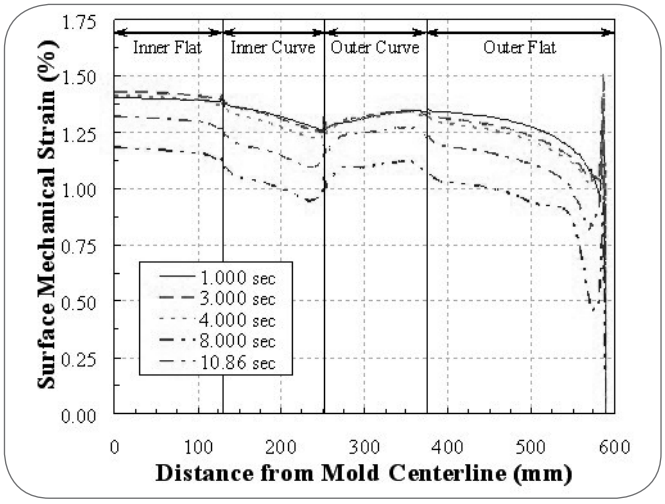

Fig. 16

Mechanical Strain Around the Perimeter.

Deformazione meccanica intorno al perimento.

ges of up to 3 °C. However, an investigation using the model revealed that the changes in the mechanical results (e.g. 0.15 MPa stress variations) caused by this two-dimensional heat transfer is less than the noise induced by mesh resolution issues in the 2D simulation. Much more important are the mechanical effects of friction at the shell surface, and bending as the shell navigates through the funnel.

The surface stresses, and corresponding strains, vary around the perimeter according to the bending of the shell caused by the funnel shape. As shown in Fig. 15, the stress changes sharply at the transitions in curvature of the funnel, especially between the inner and outer curves. Corresponding changes in strain are observed in Figs. 16, 17, and 18. Not considering the corner region, the greatest compression stress is produced at the surface of the inner curve, and is indicated by the more compressive elastic strain at the same location. The shell attempts to slide around the curved surface of the funnel as it shrinks, to alleviate stress buildup. However, this localized region of high compression extends through most of the shell thickness. Also considering the accompanying tensile region in the outer curve, this suggests that friction against the mould walls is preventing the shell from sliding as much as it wants. This results in a localized "bunching up" of the steel, which can supply the extra perimeter length that comprises a depression. Finally, significant variations are produced at the corner due to multi-dimensional effects, which may contribute to a variety of corner and off-corner defects which are not investigated in this paper.

LOCAL DEPRESSION FORMATION

Next, the model was applied to simulate the formation of a depression, initiated by local heat transfer variations at the meniscus. The location was chosen to be in the inner curve region of the funnel, given the proclivity for depression formation in that area. The applied heat flux on the shell surface was linearly decreased to 50% of the nominal values and then linearly increased back to 100% of the nominal value over a 30 mm region of the perimeter surface, centered at 175 mm from the mould centerline. Physically, this situation could occur from a finger of slag getting captured between the shell and mould during a level fluctuation.

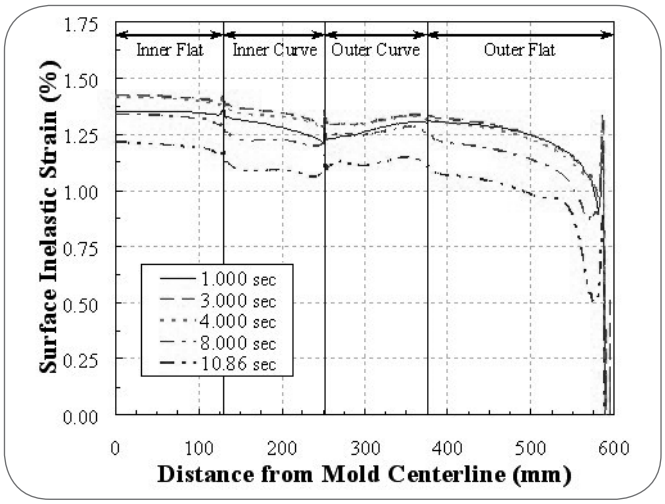

Fig. 17

Inelastic Strain Around the Perimeter.

Deformazione anelastica intorno al perimetro.

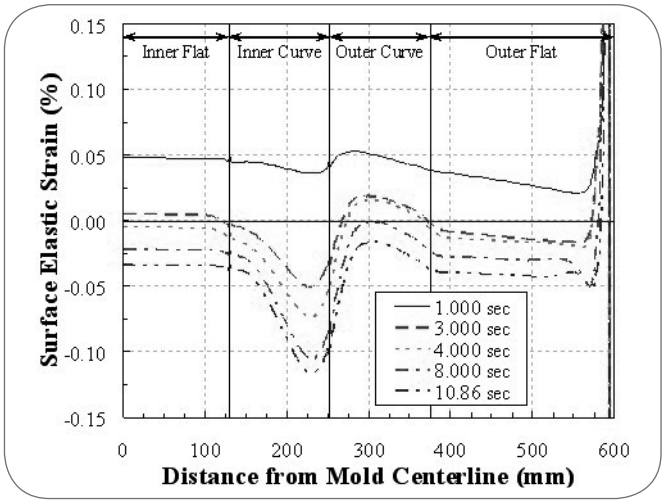

Fig. 18

Elastic Strain Around the Perimeter.

Deformazione elastica intorno al perimetro.

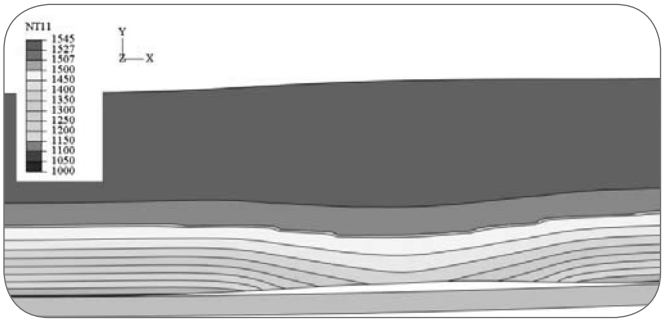

Fig. 19

Temperature Contours of Simulated Longitudinal Depression.

Profili di temperatura della depressione longitudinale simulata.

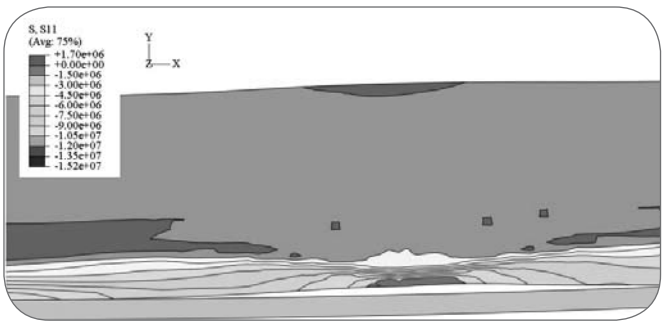

Fig. 20

Tangential Stress Contours of Simulated Longitudinal Depression.

Profili di tensione tangenziale della depressione longitudinale simulata.

Fig. 19 shows the resulting temperature contours at 7 seconds into the simulation (about 750 mm below meniscus). The heat flux drop causes a thinner shell with a hotter surface at that location. Specifically, the shell thickness decreases by 2 mm (about 20%) and the local surface temperature increased by about 300 °C, relative to the surface away from the depression. The overall compressive stress in the inner-curve region combined with the reduced shrinkage of the local hot spot causes buckling of the shell and formation of a significant gap (depression). The gap grows with distance down the mould, reaching almost 1 mm by this time. This justifies the continued heat flux drop below the meniscus. In reality, growth of the gap accompanies further drop in heat flux, which is an instability first proposed by Richmond [21]. Shortly after Fig. 19, the gap size starts to decrease, as the increasing temperature at the depression root expands to start closing the gap.

A snapshot of the accompanying tangential stress contours in the calculated depression, Fig. 20, shows that the surface of this region is under higher compression than the rest of the shell. Nearly the entire thickness of the shell in the depression is under compression, which causes the local buckling. The compression also makes it unlikely for longitudinal cracks to initiate at this time.

It is expected that depressions initiated at other locations around the perimeter would grow more slowly, owing to less bending, less compressive stress and less potential for buckling. This explains the prevalence of depressions observed in the inner-curve portion of the funnel. The compression stress appears to prevent cracks opening until below mould exit. Without mould containment, hoop tensile stress from the internal ferrostatic pressure may cause stress concentration within the hot, thin shell at the depression, leading to longitudinal crack formation, and breakouts.

Although the qualitative behavior of the gap is consistent with the measurements of an actual depression, given in Fig. 21, the actual shape of the depression computed in this work is much more shallow. The actual depression is very deep and steep, which suggests that either a slag rim variation caused the deep depression directly at the meniscus, or that further deformation causing necking of the shell is responsible for the actual depression. More work is needed to uncover the exact mechanism that causes these defects.

ANALYTICAL BENDING MODEL

The results in the previous section suggest that local gaps forming in the inner-curve region of the funnel have more chance to grow into depressions, due to the extra surface compression caused by the funnel in this region. Because stress varies greatly with temperature and strain rate, strain is a more important indicator of depression and crack danger during solidification. The strain effects observed in Figs. 16-18 can be explained by a combination of the 1D strains discussed in Figs. 11 and 12 and the bending caused by the funnel.

The bending effect, which is clearly of great importance to longitudinal defect formation, can be estimated very accurately using elementary beam bending theory [8]. Specifically, an elastic solution assuming normal strains are zero in the two non-axial directions of the beam gives the following relationship for strain through the shell thickness:

$$\varepsilon_x = -\frac{y}{r^*} \qquad (6)$$

where ε_x is the normal strain along the axis of the beam, γ is the distance from the neutral bending axis in a transverse slice (half of the shell thickness), and r^* is the local radius of curvature of the bent shape. This equation to predict mechanical strain,

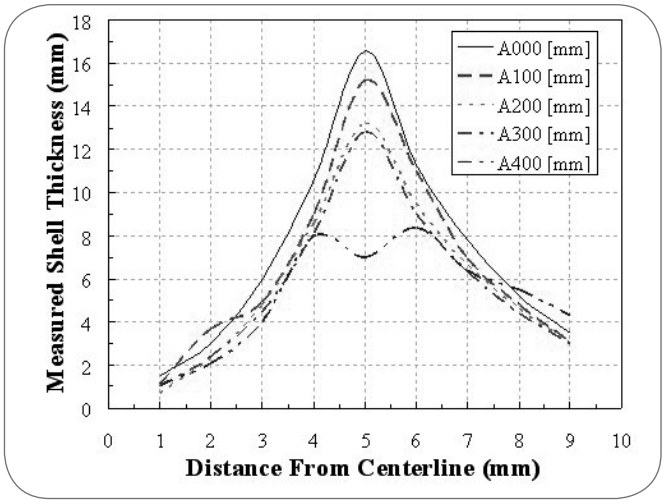

Fig. 21

Measured Longitudinal Depression Shape in a Breakout.

Forma della depressione longitudinale misurata in un difetto reale.

(consisting only of elastic strain in this case), is valid for small deflections and slope changes, such as encountered in funnel moulds. The simple relation indicates that higher strains are caused by regions of greater shell thickness and smaller radius of curvature, which accompany relatively sharp shape changes. The radius of curvature of the funnel depends only on the three parameters which define the geometry:

$$r(z) = \frac{\text{crown}(z)}{4} + \frac{(\text{funnel width} - \text{inner flat width})^2}{16 \cdot \text{crown}(z)}$$

Applying this simple model to the funnel mould of this work, (750 mm funnel width, 260 mm inner flat width, and 23.4 mm crown at the top of the mould), the radius of curvature is about 650 mm. The strain developed in bending a 10 mm shell (the approximate shell thickness at mould exit) into this shape, reaches a maximum of 0.77% on the surface in the transition region. The surface strain along the perimeter is shown in Fig. 22, and is qualitatively similar to the stresses and strains presented in Figs. 15-18. The plot of bending strains on the solidification front looks exactly the same as Fig. 22, except with the signs switched. The opening of the funnel into a flat region by mould exit causes the bend radius to increase, which induces compressive strain at the shell surface within the inner-curve region. In the absence of friction, it also induces extra tensile strain at the solidification front in the inner curve region, which would be of consequence to hot tearing.

Assuming the same 10 mm beam (shell) thickness, the model is readily applied to investigate the effect of funnel geometry on the mechanical bending strain, as shown in Fig. 23. The induced strains increase almost linearly with the crown size for a given funnel width. They decrease with increasing horizontal funnel radius. These two facts suggest that a larger funnel radius reduces the bending effect, with the limiting case of no extra bending for a parallel-sided mould. This implication can be extended to suggest that sensitivity to depression-type longitudinal facial cracks can be reduced by widening the funnel and/or decreasing the crown.

The model derivation assumes bending of a beam that is initially straight, but a simple numerical study using elastic plane stress finite elements verified that the "un-bending" behavior of the shell in a funnel mould produces almost identical results, except for small radii of curvature, where the small strain assumption breaks down. Fig. 23 includes the results of the numerical study, where all three cases (analytical, bending, unbending) match well. The numerical model also shows a more gradual transition between the neutral, tensile, and compressive regions on the surface in Fig. 22.

The bending strain increases with time down the mould as the shell thickness and funnel radius change. This effect is also observed in the 2D funnel simulations (see Figs. 15-18). In the worst case, the extra compression generated in the inner-curve region aggravates local buckling of the steel shell, which increases the likelihood of a depression type longitudinal face crack in this region.

CONCLUSIONS

A computational model of thermo-mechanical behavior of the steel shell solidifying in a funnel mould has been developed and applied to investigate the formation of longitudinal depressions and cracks. The model has been validated with analytical solutions and matches observations of longitudinal depressions in the plant. Specific conclusions arising from this work are:

1) Longitudinal depressions are more likely to grow into detrimental longitudinal facial cracks and breakouts in the inner-curve region of the steel shell in funnel-mould thin-slab casters.
2) A wider funnel and/or shallower crown increases funnel radius and helps to decrease the sensitivity to depression-type longitudinal facial cracks.
3) The two-dimensional heat transfer caused by the funnel has negligible effect on the mechanical behavior of the steel shell.
4) Increased mould lubrication should allow more uniform shrinkage of the shell, especially around the funnel region, which is so prone to longitudinal depressions.

ACKNOWLEDGEMENTS

The authors wish to thank members of the Continuous Casting Consortium at the University of Illinois at Urbana-Champaign (UIUC) for financial support, the National Center for Supercomputer Applications (NCSA) at the UIUC for computational resources, Dr. Seid Koric of NCSA, and personnel at the Corus Direct Sheet Plant in IJmuiden, The Netherlands.

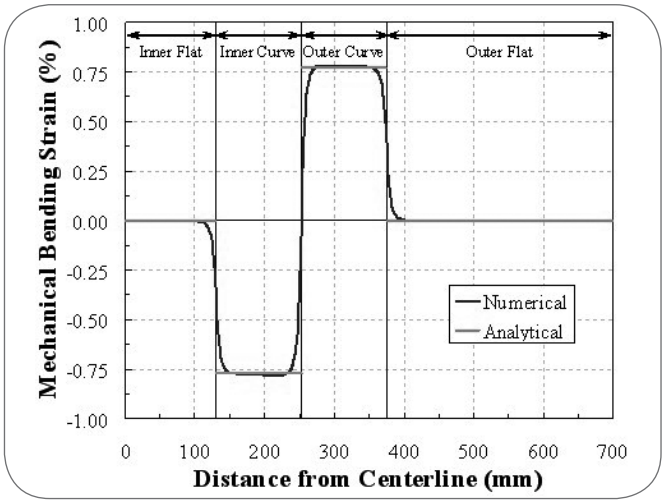

Fig. 22

Simple Bending Model Strain.

Deformazione semplice del modello di flessione.

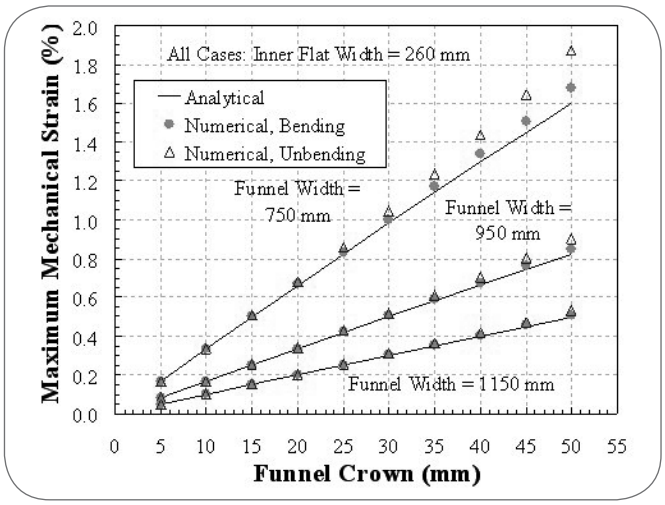

Fig. 23

Bending Strain vs. Funnel Crown.

Deformazione da flessione in rapporto alla testa dell'imbuto.

REFERENCES

1] ABAQUS User Manuals v6.7, Simulia Inc., (2007).
2] J.K. BRIMACOMBE, F. WEINBERG, and E.B. HAWBOLT, Metallurgical Transactions B, 10, (1979), p.279.
3] J.E. CAMPORREDONDO S., A.H. CASTILLEJOS E., F.A. ACOSTA G., E.P. GUTIÉRREZ M., and M.A. HERRERA G., Metallurgical Transactions B, 35, (2004), p.541.
4] K. HARSTE, Ph.D. Thesis, Technical University of Clausthal, (1989).
5] K. HARSTE, A. JABLONKA, and K. SCHWERDTFEGER, Proc. 4th Int. Conf. on Cont. Casting, Brussels, Belgium, (1988), p.633.
6] Y. HEBI, Y. MAN, Z. HUIYING, and F. DACHENG, ISIJ Int., 46, (2006), p.546.
7] L.C. HIBBELER, S. KORIC, K. XU, B.G. THOMAS, and C. SPANGLER, Proc. AISTech 2008, Pittsburgh, Pennsylvania, (2008).
8] R.C. HIBBELER, Mechanics of Materials, Prentice Hall, Upper Saddle River, New Jersey (2003).
9] H.D. HIBBITT, Nuclear Engineering and Design, 77, (1984), p.271.
10] I. JIMBO and A.W. CRAMB, Metallurgical Transactions B, 24, (1993), p.5.
11] J. KONISHI, M. MILITZER, J.K. BRIMACOMBE, and I.V. SAMARASEKERA, Metallurgical Transactions B, 33, (2002), p.413.
12] S. KORIC, L.C. HIBBELER, and B.G. THOMAS, Int. J. Num. Meth. Eng., (2008), Submitted for Review.
13] S. KORIC and B.G. THOMAS, Int. J. Num. Meth. Eng., 66, (2006), p.1955.
14] P.F. KOZLOWSKI, B.G. THOMAS, J.A. AZZI, and H. WANG, Metallurgical Transactions A, 23, (1992), p.903.
15] J.-E. LEE, T.-J. YEO, K.H. OH, J.-K. YOON, and U.-S. YOON, Metallurgical Transactions A, 31, (2000), p.225.
16] C. LI and B.G. THOMAS, Metallurgical Transactions B, 35, (2004), p.1151.
17] T.G. O'CONNOR and J.A. DANTZIG, Metallurgical Transactions B, 25, (1994), p.443.
18] J.-K. PARK, B.G. THOMAS, and I.V. SAMARASEKERA, Ironmaking Steelmaking, 29, (2002), p.359.
19] Y. MENG, B.G. THOMAS, A.A. POLYCARPOU, A. PRASAD, and H. HENEIN, Canadian Metallurgical Quarterly, 45, (2006), p.79.
20] H. MIZUKAMI, K. MURAKAMI, and Y. MIYASHITA, J. Iron Steel Inst. Japan, 63, (1977), p.S-652.
21] O. RICHMOND, in The Mathematical and Physical Modeling of Primary Metals Processing Operations (J. Szekely, J.W. Evans, and J.K. Brimacombe, eds.), TMS, Warrendale, Pennsylvania, (1988), 3-8.
22] B. SANTILLANA, B.G. THOMAS, A. HAMOEN, L.C. HIBBELER, A. KAMPERMAN, and W. VAN DER KNOOP, Proc. AISTech 2007, Indianaoplis, Indiana, (2007), p.25.
23] T. SUZUKI, K.H. TACKE, K. WUNNENBERG, and K. SCHWERDTFEGER, Ironmaking Steelmaking, 15, (1988), p.90.
24] J.H. WEINER and B.A. BOLEY, J. Mech. Phys. Solids, 11, (1963), p.145.
25] Y.-M. WON and B.G. THOMAS, Metallurgical Transactions A, (2001), p.1755.
26] P.J. WRAY, Metallurgical Transactions A, 13, (1982), p.125.
27] H. ZHU, Ph.D. Thesis, University of Illinois at Urbana-Champaign, (1993).

ABSTRACT

STUDIO DELLE CRICCHE LONGITUDINALI DI SUPERFICIE MEDIANTE MODELLI TERMOMECCANICI NELLE LINGOTTIERE A IMBUTO PER BARRE SOTTILI

Parole chiave: acciao, colata continua, modellazione

Nel presente documento sono state studiati le depressioni longitudinali e le cricche superficiali in acciaio colato in continuo in lingottiere a imbuto (lingottiere tipo "funnel") utilizzando un modello a elementi finiti per simulare il comportamento termomeccanico del guscio di solidificazione negli stampi dell'impianto di colata per barre sottili presso lo stabilimento Corus Direct Sheet Plant (DSP) di IJmuiden,Paesi Bassi. Il codice commerciale ABAQUS [1] viene utilizzato per studiare l'effetto della forma ad imbuto sulle tensioni sviluppate entro una sezione bidimensionale trasversale al guscio mentre esso si muove attraverso la lingottiera. Il modello simula prima il trasferimento di calore, basato su profili di flusso di calore rilevati in impianto mediante numerose misurazioni dell'andamento della rimozione di calore dallo stampo, con termocoppie incorporate nelle sue pareti. Questo include il calo nel flusso di calore dovuto al ritiro locale /oppure/alla formazione locale di un distacco dalla parete. La determinazione della temperatura viene immessa nel modello meccanico che include il comportamento elastico-viscoplastico dipendente dal grado dell'acciaio, dalla pressione ferrostatica, dall'inclinazione, dalle oscillazioni delle pareti dello stampo e dal contatto con le pareti sagomate dello stampo. I risultati sono stati validati mediante misurazioni nell'impianto, compresi un breakout del guscio e statistiche di criccatura. Il modello è stato applicato per poter studiare gli effetti dell'aumento della velocità di colata e della forma della lingottiera al fine di evitare cricche longitudinali.